Binary [Hydrotris(indazol-1-yl)borato]metal Complexes, $M(Tp^{4Bo})_2$[1] with M = Fe, Co, Ni, Cu, and Zn: Electronic Properties and Solvent-Dependent Framework Structures through C−H•••π Interactions

Christoph Janiak,*[a] Savaş Temizdemir,[a] Sebastian Dechert,[b] Werner Deck,[a] Frank Girgsdies,[b] Jürgen Heinze,[c] Mario J. Kolm,[a] Tobias G. Scharmann,[b] and Oliver M. Zipffel[b]

Dedicated to Prof. Dr. Heinrich Vahrenkamp on the occasion of his 60th birthday

Keywords: Boron / N ligands / UV/Vis spectroscopy / Cyclic voltammetry / Mössbauer spectroscopy / π interactions

The bis[hydrotris(indazol-1-yl)borato]metal complexes $[M\{HB(C_7H_5N_2)_3\}_2]$, $M(Tp^{4Bo})_2$, with M = Fe, Co, Ni, Cu, and Zn have been synthesized and characterized by NMR, IR, UV/Vis, MS, Mössbauer spectrometry (M = Fe) and cyclic voltammetry (M = Fe, Co). The ligand field strength of the Tp^{4Bo} ligand is slightly higher than that of the normal Tp ligand. The molecular and crystal structure of the compounds with different solvents of crystallization (tetrahydrofuran, chloroform, dioxane) were elucidated by X-ray crystallography. The metal complexes exhibit the usual pseudo-octahedral D_{3d}-symmetrical geometry for two tripodal ligands with a Jahn–Teller distortion for M = Cu. The crystal packing between the molecular complexes is controlled mainly by C–H•••π interactions from the indazolyl moieties. This gives rise to large non-covalent framework structures with voids and channels ranging in volume from about 19 to 39% of the unit cell volume. The open space is filled by solvent molecules. The crystal packing and the space group depends on the type of solvent.

Introduction

The hydrotris(pyrazolyl)borate (Tp) ligand **1** was introduced into coordination chemistry by Trofimenko more than 30 years ago[2], and in various substituted forms has developed into one of the most versatile tripodal auxiliary ligands in (bio)inorganic coordination chemistry.[3−5] Particular interest is sometimes devoted to special azolyl rings, such as triazolyl,[6−9] tetrazolyl,[10] 3,5-bis(trifluoromethyl)-pyrazolyl,[11] and indazolyl.[12,13] Poly(indazolyl)borate systems are of interest because of the possible regioisomeric structures **2a** and **2b**. The latter isomer **2b** is the empirically expected form where B−N bond formation (from KBH_4 and indazole) had occurred at the least-hindered nitrogen atom N2 (by indazole numbering).[12] This isomer, however, appears only to be encountered with 7-substituted indazoles.[13−15] With unsubstituted or otherwise substituted indazoles the isomer **2a** is formed, probably because of electronic reasons. In **2a**, boron is bonded to the sterically more hindered but electronically richer nitrogen atom.[12,16,17]

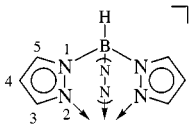

1, Tp

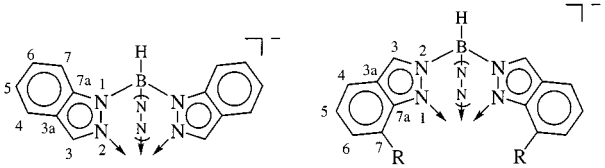

2a, Tp^{4Bo} [1] **2b, Tp^{3Bo}**

-(N-N)- denotes the third pyrazolyl or indazolyl ring which is oriented to the rear

In the extension of our work on [hydrotris(triazolyl)borato]metal complexes,[6,7,9] we were interested in the electronic ligand field effect of the anellated benzo ring on the nitrogen−metal bond.[7,18] We therefore synthesized the homoleptic bis[hydrotris(indazol-1-yl)borato]metal(II) complexes $[M(\mathbf{2a})_2]$ or $[M(Tp^{4Bo})_2]$ of iron, cobalt, nickel, copper, and zinc, to compare their electronic properties with those of the analogous bis[hydrotris(pyrazolyl)borato]-metal compounds.[19−21] Furthermore, during the course of

[a] Institut für Anorganische und Analytische Chemie, Universität Freiburg,
Albertstraße 21, 79104 Freiburg, Germany
E-mail: janiak@uni-freiburg.de
[b] Institut für Anorganische und Analytische Chemie, Technische Universität Berlin,
Straße des 17. Juni 135, 10623 Berlin, Germany
[c] Institut für Physikalische Chemie, Universität Freiburg,
Albertstraße 21, 79104 Freiburg, Germany

Supporting information for this article is available on the WWW under http://www.wiley-vch.de/home/eurjic or from the author.

  1434−1948/00/0606−1229 $ 17.50+.50/0

our studies we became interested in the crystal packing of the $M(Tp^{4Bo})_2$[1] complexes.

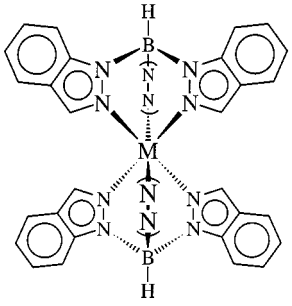

$[M(2a)_2]$, $[M(Tp^{4Bo})_2]$

-(N-N)- denotes the third indazolyl ring which is oriented to the rear or front, respectively

Syntheses and Properties of $[M\{HB(C_7H_5N_2)_3\}_2]$, $[M(Tp^{4Bo})_2]$ with M = Fe (4), Co (5), Ni (6), Cu (7), and Zn (8)

The hydrotris(indazol-1-yl)borato anion **2a** in the form of its potassium salt **3** reacts with transition-metal(II) salts in methanol with the formation of bis[hydrotris(indazol-1-yl)borato]metal(II) complexes [Equation (1)]. Yields were above 50%. The complexes are initially obtained as powders, but could be crystallized from tetrahydrofuran (THF), dioxane or chloroform. Crystallization proceeded either by slow solvent evaporation, cooling or overlayering of the dioxane phase with petroleum ether (30/50). The crystals of **4**−**8** quickly eliminate the incorporated $CHCl_3$ and THF solvent, when taken out of the solvent phase, with concomitant loss of crystallinity. The complexes are air-stable, but decompose in water. The tris[(indazolyl)borato]metal complexes are insoluble to slightly soluble in methanol and DMSO, and rather soluble in THF. The thermal stability of all compounds is high, their melting or decomposition point is above 300 °C (undetermined). A melting point of 446 °C had been determined for **4** by DSC.[12] The infrared spectra of the complexes are similar to each other, and to the potassium salt **3**.

$$MX_2 + 2\,KTp^{4Bo} \rightarrow [M(Tp^{4Bo})_2] + 2\,KX \qquad (1)$$

3

	M	X
4	Fe	$(SO_4)_{1/2}$
5	Co	Cl
6	Ni	Cl
7	Cu	Cl
8	Zn	O_2CCH_3

NMR Spectroscopy

The ^1H- and ^{13}C-NMR chemical shifts of the borato anion **2a** and of the diamagnetic transition-metal complexes correspond roughly to the spectrum of indazole[22] and of the tetrakis(indazol-1-yl)borato anion, $[B(C_7H_5N_2)_4]^-$,[16] and the signals were assigned accordingly. Despite its paramagnetism, the cobalt compound **5** gave a well-resolved ^1H-NMR spectrum with relatively sharp signals in a chemical shift range of over 200 ppm.[12]

The purity of the starting material **3** was checked by ^{11}B-NMR spectroscopy, and small impurities of unreacted KBH_4 as well as presumably the intermediate dihydrobis(indazolyl)borato anion, were detected.

Mass Spectrometry

The mass-spectrometric characterization shows the molecular ion for all the complexes. The Jahn−Teller-distorted Cu complex **7** gives, however, a significantly lower molecular ion intensity, and apparently also an immediate loss of one hydrogen. The most likely fragmentation for the bis[hydrotris(indazolyl)borato]metal(II) complexes involves the loss of indazolyl or indazole rings ($C_7H_5N_2$/H) and the loss of one hydrotris(indazolyl)borato ligand. The occurrence of doubly charged ions of high abundance is remarkable. The typical fragments together with their proposed fragmentation path are given in Scheme 1. For iron and cobalt, the doubly charged ion that was obtained after the loss of two indazolyl rings, $[M - 2\,(C_7H_5N_2)]^{2+}$, even represented the base peak. Figure 1 shows the mass spectrum of the iron complex **4** together with its assignment, as an example.

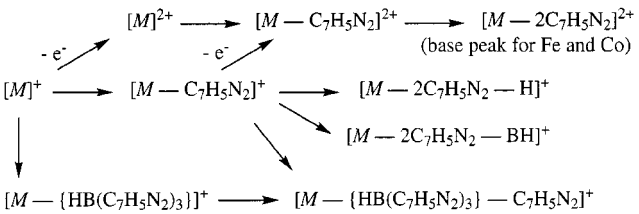

Scheme 1. Typical fragments in the mass spectra of the $[M\{HB(C_7H_5N_2)_3\}_2]$ complexes and proposed fragmentation path (*M in italics* = molecular complex)

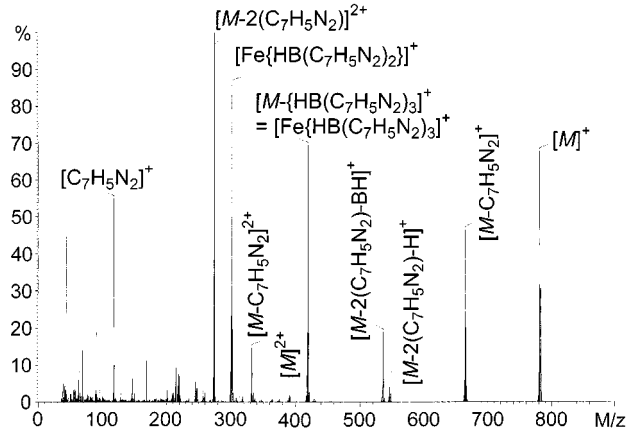

Figure 1. Mass spectrum of **4** with assignment; peak assignment was based on the calculation of the most abundant isotope combination, containing ^{56}Fe and ^{11}B; note the doubly charged ions

Optical Spectra

The positions of electronic absorption maxima and the extinction coefficients for the complexes **4**−**7** are given in Table 1 together with the assignments. The optical spectra of the complexes feature weak d-d transitions and strong metal-to-ligand charge-transfer (CT) bands. The latter start

Table 1. UV/Vis data of **4**–**7**

Complex[a]	λ [nm]	$\tilde{\nu}$ [cm^{-1}]	ε	Assignment[b]	Comparison λ [nm] for $[M\{HB(pz)_3\}_2]$ and $[M\{HB(tz)_3\}_2]$[c]	
4	493	20 280	238	$^1A_{1g} \rightarrow {}^1T_{1g}$	535[d]	526[e]
5	877	11 400	1.7	$^4T_{1g} \rightarrow {}^4T_{2g}$	901[f][g]	n.o.[e][h]
	n.o.			$(^4T_{1g} \rightarrow {}^2T_{2g}, {}^2T_{1g})$	641	n.o.
	449	22 270	75 (sh)	$^4T_{1g} \rightarrow {}^4A_{2g}$	515 (sh)	509
	425	23 530	109	$^4T_{1g} \rightarrow {}^4T_{1g}$ (P)	459	450
	404	24 810	114	$(^4T_{1g} \rightarrow {}^2A_{1g})$	n.o.	n.o.
6	776	12 890	20	$^3A_{2g} \rightarrow {}^3T_{2g}$	849[g]	
	700	14 290	11(sh)	$(^3A_{2g} \rightarrow {}^1E_g)$	760 (sh)	
	504	19 840	25	$^3A_{2g} \rightarrow {}^3T_{1g}$	570	n.a.[h]
	429	23 310	16 (sh)	$(^3A_{2g} \rightarrow {}^1T_{1g})$	522	
	389	25 710	38 (sh)	$(^3A_{2g} \rightarrow {}^1A_{1g})$	450	
	n.o., CT			$^3A_{2g} \rightarrow {}^3T_{1g}$ (P)	334	
7	633	15 790	9	$^2E_g \rightarrow {}^2T_{2g}$ (O_h)	620[g]	630[e]
				$^2B_{1g} \rightarrow {}^2B_{2g}$, ^2E_g (D_{4h})		

[a] All complexes measured in $CHCl_3$; concentrations: **4** 4.7•10^{-3} mol•l^{-1}, **5** 6.0•10^{-3} mol•l^{-1}, **6** 10.2•10^{-3} mol•l^{-1}, **7** 2.9•10^{-3} mol•l^{-1}. – [b] Term symbols are taken for octahedral complexes, thereby assuming a near to O_h site symmetry at the metal center. Although it is recognized that the actual complex symmetry is D_{3d}. Parentheses indicate spin-forbidden transitions. – [c] pz = pyrazolyl, tz = triazolyl. – [d] J. P. Jesson, S. Trofimenko, D. R. Eaton, *J. Am. Chem. Soc.* **1967**, *89*, 3158–3164. – [e] C. Janiak, *Chem. Ber.* **1994**, *127*, 1379–1385. – [f] J. P. Jesson, *J. Chem. Phys.* **1966**, *45*, 1049–1056. – [g] J. P. Jesson, S. Trofimenko, D. R. Eaton, *J. Am. Chem. Soc.* **1967**, *89*, 3148–3158. – [h] n.o. = not observed, n.a. = not available.

at 340 nm. Hence, the highest energetic spin-allowed transition for the nickel complex **6**, $^3A_{2g} \rightarrow {}^3T_{1g}$ (P), could not be observed. The spectra are related to those of the analogous bis[hydrotris(pyrazolyl)borato]- and bis[hydrotris(triazolyl)-borato]metal compounds.[18–21] Data for comparison is included in Table 1. It is evident that corresponding bands for the indazolyl complexes are shifted to lower wave length by about 25 to 70 nm for most transitions. This shift to higher energy can be correlated to a stronger ligand field of the tris(indazolyl)borato anion versus the tris(pyrazolyl)borato analog. The ligand-field strength can be quantified by the *f* value relative to H_2O (*f* = 1.00). The value *f* is calculated from $\Delta_O = f \times g$(central ion).[23] The Ni^{II} transition $^3A_{2g} \rightarrow {}^3T_{2g}$ corresponds to Δ_O = 12890 cm^{-1}. Together with $g(Ni^{2+})$ = 8900 one obtains *f* = 1.45 for hydrotris(indazolyl)borate, which is slightly larger than *f* = 1.35 for hydrotris(pyrazolyl)borate.[20] Both ligands are stronger than 2,2′-bipyridine (*f* = 1.33) or ammonia (*f* = 1.25). We note that the copper complex **7** does not follow the aforementioned hypsochromic shift.

Electrochemistry of 4 and 5

The cyclic-voltammetric investigations on the (indazolylborato)iron and -cobalt complex **4** and **5**, respectively, can be compared to the data available for the iron and cobalt analog with the hydrotris(pyrazolyl)borato and the hydrotris(triazolyl)borato ligand.[8] The results are collected in Table 2. The cyclic voltammograms for **4** and **5** are shown in Figure 2. Based on the difference of the peak potentials, ΔE_p, the iron complex **4** exhibits a reversible and fast electron transfer. The electron processes for the cobalt complex **5** are only quasi-reversible and slow. This agrees with the behavior found for the respective tris(pyrazolyl)borato derivatives. It is suggested that the slow electron transfer for cobalt is due to different spin states for Co^{II} (high spin) and Co^{III} (low spin). In comparison with the (pyrazolyl)- and (triazolyl)borato complexes, the potentials of **4** lie at intermediate values. Hence, the [(indazolyl)borato]iron complex is more difficult to oxidize than the pyrazolyl analog, but easier to oxidize than the triazolyl compound. Whereas the cobalt complex **5** is easier to oxidize than its pyrazolyl congener. This may seem contradictory at first, but the phenomena can be explained with the slightly stronger ligand field of **Tp^{4Bo}** versus **Tp** according to Scheme 2. An increase in the σ-donor and π-acceptor strength increases the ligand-field splitting. In octahedral symmetry (assumed for simplicity), the t_{2g} levels are lowered, the antibonding e_g levels raised in energy. The d^6-Fe^{II} complex **4** is low spin with the electron configuration $t_{2g}{}^6$. Thus, it becomes more difficult

Table 2. Summary of voltammetric parameters for the oxidation of $[M\{HB(azolyl)_3\}_2]$, M = Fe, Co; azolyl = pyrazolyl, triazolyl, indazolyl

Complex[a]	E_{pc}/mV[b]	E_{pa}/mV[b]	$E_{1/2}$/mV[c]	ΔE_p/mV[d]	n[e]	Remarks
$[Fe\{HB(pyrazolyl)_3\}_2]$	139	232	185.5	93	1.03	Ref.[8], reversible one-electron process
$[Fe\{HB(indazolyl)_3\}_2]$ (**4**)	490	580	530	90		Reversible one-electron process
$[Fe\{HB(triazolyl)_3\}_2]$	810	1031	920.5	221	0.67	Ref.[8], quasi-reversible one-electron process
$[Co\{HB(pyrazolyl)_3\}_2]$	−217	213	4	430	0.93	Ref.[8], quasi-reversible one-electron process
$[Co\{HB(indazolyl)_3\}_2]$ (**5**)	−110	100	0	210		Quasi-reversible one-electron process
$[Co\{HB(triazolyl)_3\}_2]$	641	811	726	170	1.27	Ref.[8], quasi-reversible one-electron process

[a] Supporting electrolyte 0.1 mol/l $[nBu_4N][ClO_4]$ or $[nBu_4N][PF_6]$; *T* = 25 °C, solvent CH_2Cl_2, complex concentration 1•10^{-3} mol/l, reference Ag/AgCl, scan rate 100 mV/s. – [b] Cathodic and anodic potentials. – [c] $E_{1/2} = (E_{pa} + E_{pc})/2$. – [d] Difference between the anodic and cathodic peak potentials, $\Delta E_p = E_{pa} - E_{pc}$. – [e] Number of transferred electrons, $n = i_{pa}/i_{pc}$.

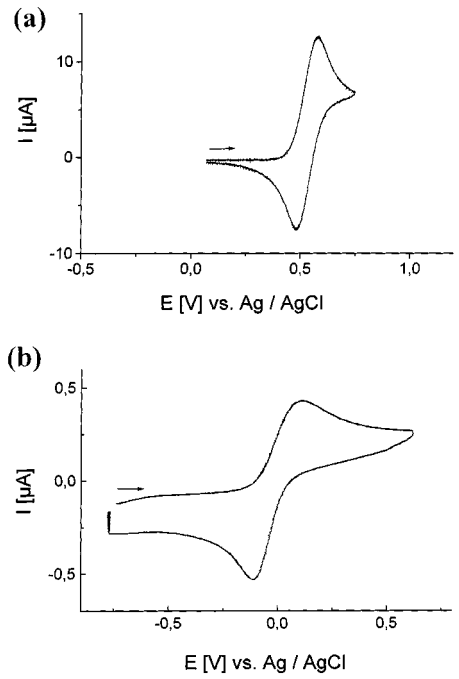

Figure 2. Cyclic voltammograms of (a) **4** and (b) **5** in CH_2Cl_2 (complex concentration 10^{-3} mol/l, 25 °C, scan rate 100 mV/s, 0.1 mol/l [nBu$_4$N][PF$_6$])

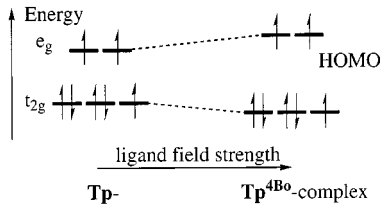

Scheme 2. The effect of an increase in ligand-field strength for Co^{II} (high spin) in O_h symmetry; from the raised e_g levels the complex becomes easier to oxidize when going from the **Tp** to the **Tp^{4Bo}** complex

to oxidize. The d^7-Co^{II} complex **5** is high spin with the electron configuration $t_{2g}^5e_g^2$. With the e_g levels raised in energy, it becomes easier to oxidize.

Mössbauer Spectroscopy of 4

Hexa-coordinated complexes of iron(II) with nitrogen donor ligands are good candidates for a temperature-induced spin crossover between the diamagnetic $^1A_{1g}$ low-spin state and the paramagnetic $^5T_{2g}$ high-spin state.[24] Also, the iron complexes of tris(pyrazolyl)borato ligands exhibit such a spin equilibrium [8,9,18,25–28] and the transition temperature was found to vary strongly with substitution on the pyrazolyl rings or the boron atom.[19,20,29] The interplay of the steric effects of substituents with the different sizes of the low- and high-spin Fe^{II} ions was demonstrated to be the decisive factor in controlling the relative stability of the spin states.[26,28] As such, we have investigated the possible spin crossover behavior of **4** by variable-temperature ^{57}Fe-Mössbauer spectroscopy. Figure 3 shows the Mössbauer spectra of **4** at three temperatures from 287 K

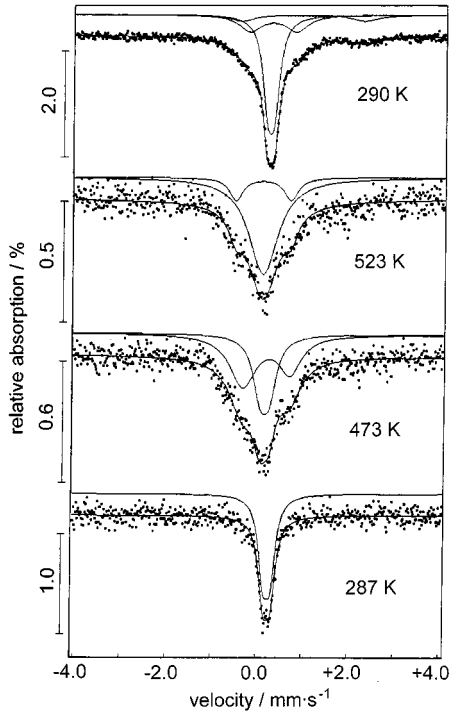

Figure 3. ^{57}Fe-Mössbauer spectra of **4** as a function of temperature; the isomer shift is scaled to the shift of α-Fe as the origin of the ordinate; the uppermost spectrum at 290 K was measured after heating the sample to 523 K and may contain some decomposition product

Table 3. Parameters of ^{57}Fe-Mössbauer spectra for the iron complex **4** (cf. Figure 3)

T/K [θ/°C]	N_{lin} [a]	$\delta^{\alpha\text{-Fe}}$[b] /mm s^{-1}	$\Gamma/2$[c] /mm s^{-1}	ΔE_Q [d] /mm s^{-1}	A_r/%[e] (A/A_Σ)
290 [17][f]	3	0.24	0.28	0.15	60
		0.28	0.61	1.02	28
		0.95	0.71	2.70	13
523 [250]	2	0.20	0.79	0.00	82
		0.20	0.38	1.21	18
473 [200]	2	0.21	0.54	-0.23	62
		0.24	0.56	1.16	38
287 [14]	1	0.34	0.26	0.16	100

[a] Number of lines used to fit the spectrum. – [b] Isomer shift refered to α-iron at room temperature. – [c] $\Gamma/2$ is half of the half-width value Γ. – [d] Quadrupole splitting. – [e]Line area relative to total area. – [f] The spectrum was measured after heating the sample to 523 K and may contain some decomposition product.

to 523 K. The corresponding Mössbauer parameters are collected in Table 3.

The initial room-temperature spectrum shows a doublet with a very small quadrupole splitting (0.16 mm s^{-1}). This, and the small positive isomer shift of 0.34 mm s^{-1}, is expected for a low-spin ($^1A_{1g}$) iron(II) complex with only a small distortion (D_{3d}) from octahedral ligand symmetry. The high-temperature spectra show a distinctly different line profile. Phenomenologically, they can be described as a broad singlet with a fine structure (shoulders). The spectra were fitted with a narrow doublet, or singlet and a wider doublet, both with a very similar isomer shift. The actual origin of the wide doublet is unclear. The small isomer shift

of 0.2 to 0.24 mm s^{-1} as well as the medium quadrupole splitting of 1.1 to 1.2 mm s^{-1} argue against iron(II) in the high-spin $^5T_{2g}$ state. Usually, for high-spin iron(II) in the quintet state an isomer shift of 0.7 to 1.2 mm s^{-1} and a large quadrupole splitting of 2.3 to 3.0 mm s^{-1} is expected.[8,24,29] Hence, we would not ascribe the fine structure to a quadrupolar relaxation phenomenon, i.e. to the onset of a spin transition. Possibly, the wide doublet may stem from partial decomposition: A second room-temperature spectrum, which was collected after heating the sample, still shows a broadened envelope around the main signal. In addition, a flat peak at positive isomer shift had emerged, which could be fitted to a doublet with an isomer shift of 0.95 mm s^{-1} and a large quadrupole splitting of 2.07 mm s^{-1}. The visual appearance of the sample was unchanged after the Mössbauer experiments.

For the bis(ligand) complex of iron with tris(pyrazolyl)borate (**1**) a transition temperature (50% low- and high-spin state) of about 133 °C was given.[26] It is suggested that the increased ligand-field strength of **2a** versus **1** may be the basis for the considerable increase in transition temperature beyond the decomposition point of the sample.

X-ray Structures of [M(Tp^{4Bo})$_2$] Complexes (M = Fe, Co, Ni, Cu, Zn) with Solvent of Crystallization

The bis[hydrotris(indazol-1-yl)borato]metal complexes could be crystallized from THF, dioxane or chloroform. The following complexes were investigated by single-crystal X-ray structure determination: **4** • 3.5 $CHCl_3$, **5** • 3.5 $CHCl_3$, **6** • 3 THF, **6** • 1.67 dioxane, **7** • 1.33 $CHCl_3$, **7** • 2.5 THF, and **8** • 1.67 dioxane. The number of solvent molecules was derived from the structure refinement. The interest in different solvents of crystallization stems from a solvent-dependent crystal packing, which became apparent in the course of these studies.

The (common) molecular structure of the M(Tp^{4Bo})$_2$ complexes for M = Fe, Co, Ni, and Zn (**4**, **5**, **6**, and **8**, respectively) is shown in Figure 4. The metal complexes exhibit the usual D_{3d}-symmetrical geometry for two tripodal ligands. In each space group found here, the metal atom occupies a center of inversion as a special position. Hence, both ligands in a complex molecule are symmetry-related. The copper compound **7** is depicted in Figure 5. The metal atoms are pseudo-octahedrally coordinated by the tris(chelate) ligand **2a**, and complex **7** exhibits the expected Jahn–Teller distortion for the d^9 ion with four short and two long Cu–N distances. The metal–nitrogen bond lengths and angles are summarized in Table 4. They are unremarkable with respect to those of other bis[tris(pyrazolyl)borato]-[30–33] and bis[tris(triazolyl)borato]metal complexes[7,18,34,35] and M–N bond lengths in general.[36] A comparison of the average M–N bond lengths from Table 4 shows the expected decrease for high-spin ions from Co to Ni, and again an increase towards Zn.[37] The rather short metal–ligand bond length for the iron compound **4** is indicative of a low-spin complex, in agreement with the Mössbauer data (see above).

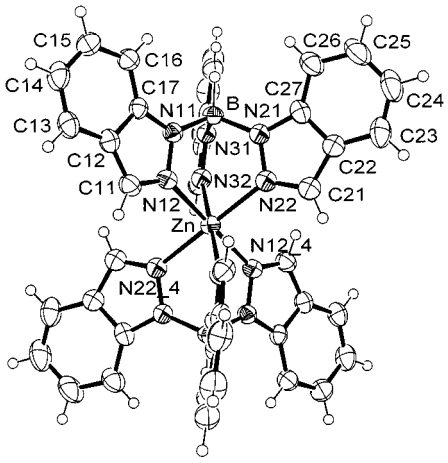

Figure 4. Molecular structure of [Zn{$HB(C_7H_5N_2)_3$}$_2$] (**8**); selected distances [Å] and angles [°]: Zn–N12 2.157(3), Zn–N22 2.156(3), Zn–N32 2.149(3); N12–Zn–N22 84.0(1), N12–Zn–N32 86.4(1), N22–Zn–N32 87.2(1), N12–Zn–N22 4 96.1(1), N32–Zn–N12 4 93.7(1), N32–Zn–N22 4 92.9(1) (see also Table 4) (symmetry-equivalent position 4 = 1 − x, −y, 1 − z)

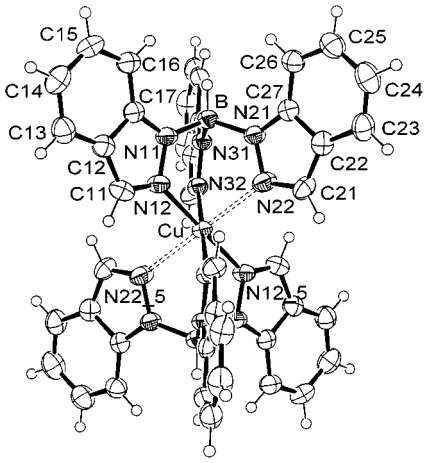

Figure 5. Molecular structure of [Cu{$HB(C_7H_5N_2)_3$}$_2$] (**7**) in **7** • 2.5 THF; selected distances [Å] and angles [°]: Cu–N12 2.043(4), Cu–N22 2.318(4), Cu–N32 2.019(3); N12–Cu–N22 86.8(1), N12–Cu–N32 87.1(1), N22–Cu–N32 85.2(1), N12–Cu–N22 5 93.3(1), N32–Cu–N12 5 92.9(1), N32–Cu–N22 5 94.9(1) (see also Table 4) (symmetry-equivalent position 5 = −x, 1 − y, −z)

One might have thought that the crystal packing of the complex molecules could be dictated by so-called face-to-face π-stacking interactions between six-membered rings of the indazolyl moieties. Such a parallel or a parallel-displaced π-stacking with a ring separation between 3.3 to 3.8 Å is an important non-covalent organization possibility in supramolecular chemistry.[38–40] Yet, the crystal packing between the molecular complexes appears to be controlled more by C–H•••π interactions from the indazolyl moieties, which is exemplified in Figure 6 and 7. Such a C–H•••π interaction between aromatic rings is referred to as a point-to-face or T-shaped arrangement.[41] Only in the structure of the nickel derivative **6** • 3 THF was a slipped face-to-face

Table 4. Selected bond lenghts and angles in the bis[hydrotris(indazol-1-yl)borato]metal complexes $M(Tp^{4Bo})_2$

Compound[a]	$Fe(Tp^{4Bo})_2$ in **4** • 3.5 $CHCl_3$[b]	$Co(Tp^{4Bo})_2$ in **5** • 3.5 $CHCl_3$[b]	$Ni(Tp^{4Bo})_2$ in **6** • 3 THF[b]	$Ni(Tp^{4Bo})_2$ in **6** • 1.67 dioxane	$Cu(Tp^{4Bo})_2$ in **7** • 1.33 $CHCl_3$[c]	$Cu(Tp^{4Bo})_2$ in **7** • 2.5 THF	$Zn(Tp^{4Bo})_2$ in **8** • 1.67 dioxane
M−N range [Å]	1.941(7)−1.972(7)	2.096(5)−2.139(5)	2.049(3)−2.066(3)	2.084(3)−2.091(4)	short: 2.002(2)−2.025(2) long: 2.357(2)−2.453(3)	short: 2.019(3) and 2.043(4) long: 2.318(4)	2.149(3)−2.157(3)
M−N average [Å]	1.958	2.117	2.058	2.087	short: 2.015 long: 2.407	short: 2.031 long: 2.318	2.154
range N−M−N chelate bite angles [°]	87.9(3)−89.5(3)	84.9(2)−86.8(2)	85.0(1)−87.7(1)	85.5(1)−87.7(1)	83.78(9)−87.66(9)	85.2(1)−87.1(1)	83.95(10)−87.15(10)
average N−M−N chelate bite angles [°]	88.6	86.1	86.5	86.9	86.0	86.4	85.8
N−M−N *cis*, except chelate [°]	90.5(3)−92.1(3)	93.2(2)−95.1(2)	92.3(1)−95.0(1)	92.3(1)−94.5(1)	92.34(9)−96.22(9)	92.9(1)−94.9(1)	92.85(10)−96.05(10)
average N−M−N *cis*, except chelate [°]	91.4	93.9	93.6	93.1	94.0	93.7	90.9

[a] Only one of the borato ligands is unique. The two borato ligands are symmetry-related through a center of inversion; special position of the metal atom. Hence, the N−M−N *trans* angles are 180.0°. − [b] Two symmetrically independent molecules in the unit cell. − [c] Three symmetrically independent molecules in the unit cell.

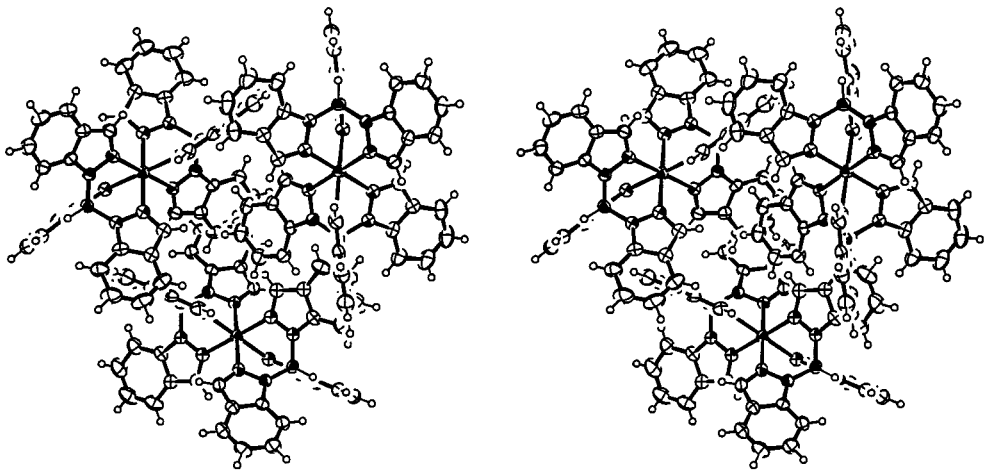

Figure 6. Stereoview of the section of the crystal structure of **4** • 3.5 $CHCl_3$ (isostructural with **5** • 3.5 $CHCl_3$) to illustrate the C−H•••π interactions between the indazolyl moieties; solvent molecules have been omitted; view approximately along *c*

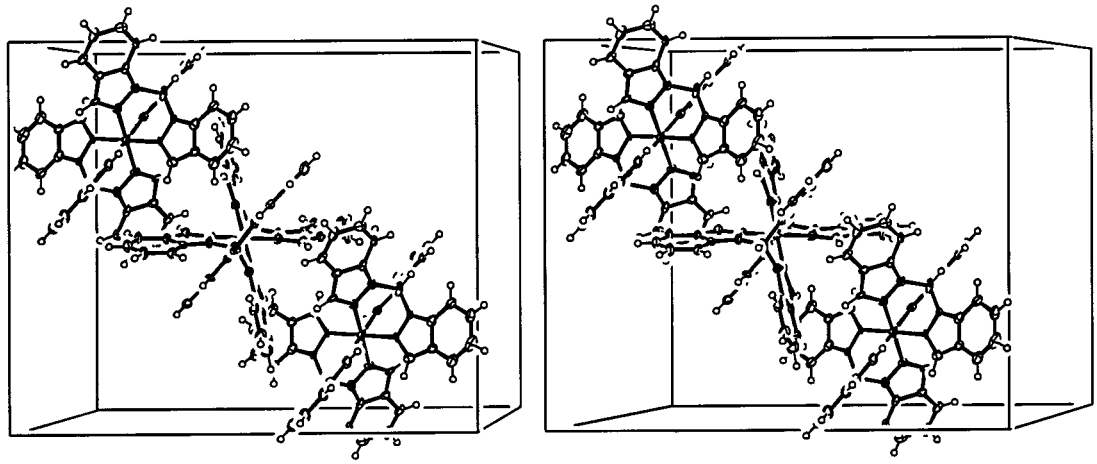

Figure 7. Stereoview of the section of the crystal structure of **8** • 1.67 dioxane (isostructural with **6** • 1.67 dioxane) to illustrate the C−H•••π interactions between the indazolyl moieties; solvent molecules have been omitted

aromatic−aromatic interaction more prominent (see Figure 9). The preference for a C−H•••π interaction can be understood when keeping in mind the fact that a parallel face-to-face geometry for aromatic rings is not necessarily attractive. For non-polarized π-systems π−π repulsion prevents a parallel π-stacking and σ−π attraction favors either a T-shaped or a displaced geometry.[42] According to the so-called Hunter−Sanders rules, a face-to-face interaction requires π-deficient and σ-positive atoms in polarized π-systems.[40,43] At the same time, a charge-charge interaction

Table 5. Potential solvent areas and C−H•••π contacts; computed with the program PLATON

Compound	**4** • 3.5 $CHCl_3$	**5** • 3.5 $CHCl_3$	**6** • 3 THF	**6** • 1.67 dioxane	**7** • 1.33 $CHCl_3$	**7** • 2.5 THF	**8** • 1.67 dioxane
Potential solvent area in solvent-free crystal lattice: volume [Å^3]/unit cell volume [Å^3]	4001.5/10362.7 ≅ 38.6%	4003.9/10490.4 ≅ 38.2%	861.3/2503.0 ≅ 34.4%	3077.7/10514.5 ≅ 29.3%	619.6/3285.3 ≅ 18.8%	1248.8/4656 ≅ 26.8%	3012.9/10536.1 ≅ 28.6%
Calculated solvent molecule volume [Å^3][a] = solvent area/number of solvent molecules (in unit cell)	4001.5/(3.5×8) = 143[a]	4003.9/(3.5×8) = 143[a]	861.3/(3×2) = 144[a]	3077.7/(1.67×9) = 205[a]	619.6/(1.33×3) = 155[a]	1248.8/(2.5×4) = 125[a]	3012.9/(1.67×9) = 201[a]
Shortest intermolecular **C−H•••C(π) contacts,** H•••C distances [Å] (and angles [°])[b][c]	2.70 (156.6)	2.77 (162.6)	2.70 (154.8)	2.81 (146.5)	2.66 (165.5)	2.89 (127.9)	2.77 (132.0)
Shortest intermolecular **ring-centroid−ring-centroid contacts** [Å] (with interplanar angle [°])[b][d]	R5−R5: 4.496 (51.3) R6−R5: 4.471 (50.0) R6−R6: 4.546 (49.7)	R5−R5: 4.803 (74.7) R6−R5: 4.435 (47.9) R6−R6: 4.493 (47.1)	R5−R5: 4.267 (7.0) R6−R5: 3.931 (6.1) R6−R6: 3.673 (6.5)	R5−R5: 4.809 (54.0) R6−R5: 4.628 (15.9) R6−R6: 4.892 (31.9)	R5−R5: 4.703 (60.7) R6−R5: 4.537 (49.8) R6−R6: 4.875 (62.2)	R5−R5: 4.942 (49.0) R6−R5: 5.190 (41.9) R6−R6: 4.913 (53.3)	R5−R5: 5.013 (57.3) R6−R5: 4.635 (24.8) R6−R6: 4.869 (31.4)
Shortest intermolecular contact (R6) **C−H•••ring-centroid** (R5 or R6) [Å][b,d]	R5: 3.18 R6: 3.08	R5: 3.03 R6: 2.66	R5: 2.96 R6: 3.15	R5: 2.85 R6: 2.79	R5: 2.70 R6: 2.65	R5: >3.4 R6: 3.08	R5: 2.87 R6: 2.76

[a] This has to be compared to an expected solvent volume for small molecules of 100−300 Å^3. − [b] A full listing of the intermolecular C−H•••π contacts [C−H•••C < 3.1 Å, C−H•••centroid < 3.4 Å (distances and angles)] and of the ring-centroid−ring-centroid contacts (< 6.0 Å) has been deposited as supporting information. − [c] The sum of the contact radii of carbon (1.70 Å) and hydrogen (1.20 Å) is 2.90 Å as given by: A.Bondi, *J. Phys. Chem.* **1964**, *68*, 441. (or covalent radius + 0.8 Å. when not given). − [d] R5 denotes the 5-membered nitrogen-containing pyrazol-type ring, R6 denotes the 6-membered anellated aryl ring of the indazolyl group.

dominates for highly charged π-systems. We suggest that delocalization of the negative ligand charge into the indazolyl rings may be the basis of a charge repulsion and C−H$^{\delta+}$−$^{\delta-}$π attraction.

The T-shaped C−H•••π interaction is found for example in the crystal structure of benzene.[44] Molecular dynamics calculations for benzene gave an optimum distance of 4.99 Å between the two ring centers in the T-shaped orientation. The theoretical interaction energy is about 10 kJ/5mol. Even at a benzene−benzene center of mass separation of 6 Å the T-shaped point-face dimer is bound by about 1.6 kJ/mol.[41,42] Table 5 summarizes the shortest intermolecular C−H•••π contacts with distances and angles. Ring-centroid−ring-centroid contacts shorter than 4.99 Å can be observed. From Figure 6 and 7 and the comparison of the interplanar angles, it is evident that the aromatic rings do not lie perpendicular to one another. Most angles are between 40 and 80° (cf. supporting information), i.e. we have tilted structures intermediate between the parallel displaced and the point-face geometry.[41] The intermolecular C−H•••π contacts start around 2.7 Å for C−H•••C and C−H•••ring centroid distances (Table 5). As such, these shortest C−H•••π contacts in the structures of **4** to **8** lie at the short end of the accepted distance range for this type of contact.[45] A full listing of the intermolecular C−H•••π contacts [C−H•••C < 3.1 Å, C−H•••centroid < 3.4 Å (distances and angles)] and of the ring-centroid−ring-centroid contacts (< 6.0 Å) can be found in the supporting information.

The solvent-incorporating structures of **4** to **8** indicate that even the very weak intermolecular C−H•••π interactions can be used to construct porous framework structures.[46] This mode of assembly gives rise to large non-covalent framework structures with voids and channels from about 19 to 39% of the unit cell volume (see Table 5). Figure 8 to 11 provide example views of these open spaces in six compounds. There, most of the potential solvent areas are built as channels. Only in the structure of **7** • 1.33 $CHCl_3$ (not shown) are cavities solely formed. The open space is filled by solvent molecules and probably based on very weak C−H•••O or C−H•••Cl hydrogen bonding. Because of the weak host−guest interactions the

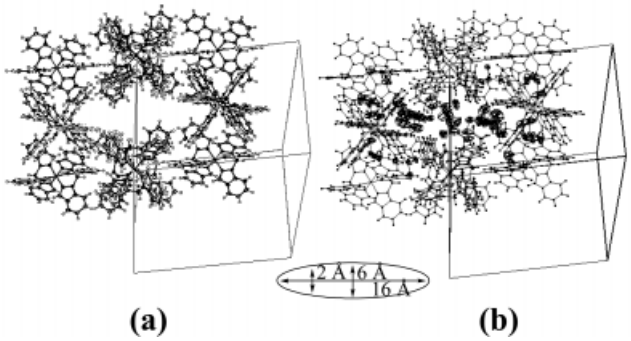

Figure 8. (a) Solvent-omitted crystal structure of **4** • 3.5 $CHCl_3$ (isostructural with **5** • 3.5 $CHCl_3$) to illustrate the channel formation along the *ab* diagonal (110 plane) and (b) the same view with a wire-frame model of the metal complexes together with the solvent molecules

solvent molecules are prone to disorder. The disorder model for the dioxane molecules in Figure 11b, which lie within the channels, is sketched in **9**. These disordered dioxane molecules give the impression of a close-packed cluster. A three-fold inversion axis ($\bar{3}$), perpendicular to the plane of projection in Figure 11 passes through them. It is suggested that the inversion axis is parallel to but does not coincide with the molecular C_2 axis bisecting the C−C bonds. The three-fold rotation wraps the molecule around with the oxygen atoms pointing outward.

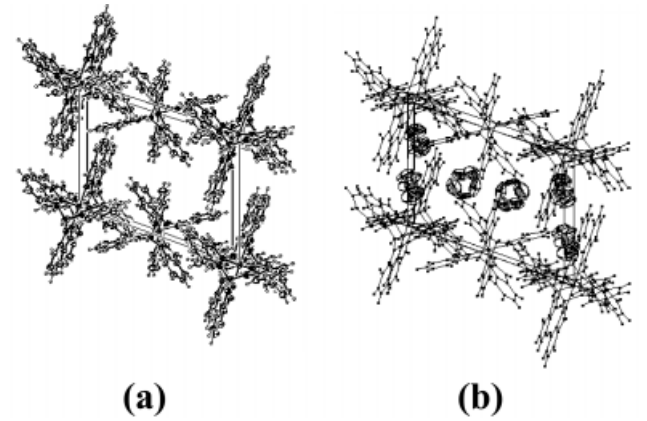

Figure 9. (a) Solvent-deleted crystal structure of **6** • 3 THF showing the channel formation along *a* and (b) the same view with a wire-frame model of the metal complexes together with the THF molecules

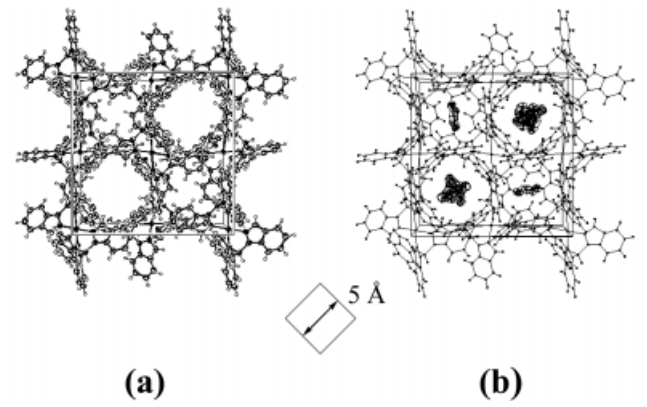

Figure 10. (a) Solvent-omitted crystal structure of **7** • 2.5 THF with the channel formation along the *c* axis and (b) the same view with a wire-frame model of the metal complexes together with the, in part, disordered solvent molecules

The calculated solvent volumes (Table 5) fall well into the expected solvent volume range of 100−300 Å^3 for small molecules. This gives some indication that the number of solvent molecules has been correctly determined within the structure refinement. The crystal packing and the space

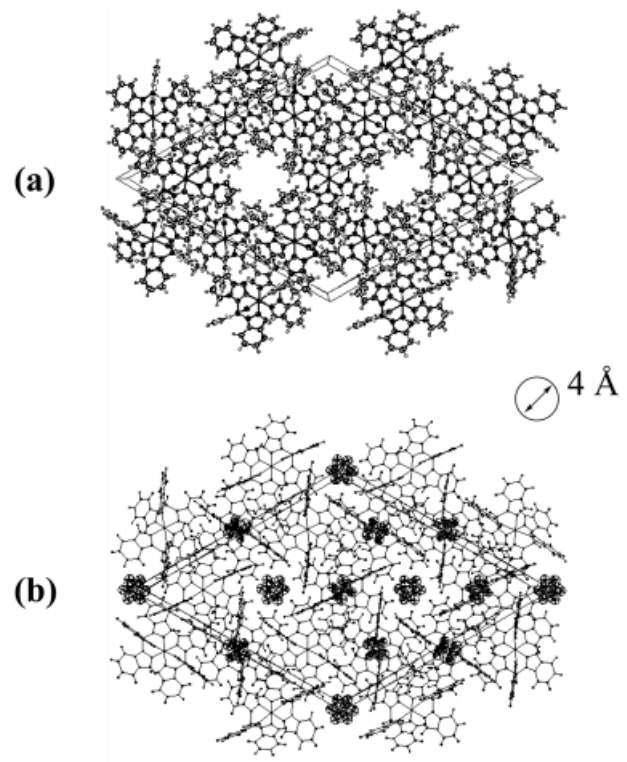

Figure 11. (a) Solvent-deleted crystal structure of **8** • 1.67 dioxane (isostructural with **6** • 1.67 dioxane) to illustrate the channel formation along *c* and (b) the same view with a wire-frame model of the metal complexes together with the disordered solvent molecules

group then depend on the type of solvent. It is well known that solvents of crystallization can have a substantial effect on the molecular and/or crystal structure of a compound.[47−49] We are currently investigating if the dioxane molecules can, at least in part, be reversibly removed from and reinserted into the framework. If so, one may envision the construction of supramolecular sensors for such small molecules in combination with a quartz crystal micro-balance.[50]

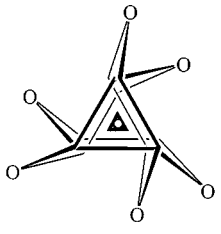

9

Conclusion

A UV/Vis-spectrometric comparison of the metal complexes shows that the tris(indazolyl)borate ligand **2a** is a somewhat stronger ligand than the long-known hydrotris(pyrazolyl)borate parent system **1**. From cyclic voltammetric studies on the iron and cobalt complexes of **2a** and **1** it is evident that the former has the effect of decreasing the energy of the t_{2g} orbitals and increasing the energy of the e_g orbitals. Unlike other homologue failed to exhibit a

temperature-induced low- to high-spin crossover before the decomposition point.

The molecular bis[hydrotris(indazolyl)borato]metal complexes can pack only loosely in the crystal leaving voids and channels which amount to as much as 38% of the unit cell volume. The voids are filled by solvent molecules. The low density packing of the molecular complexes may be due to a reluctance of the indazolyl moieties to enter into face-to-face π-stacking interactions. Instead, the crystal packing is controlled more by tilted point-face C−H•••π interactions. Most indazolyl ring planes form intermolecular angles between 40 and 80°. On the other hand, the solvent-incorporating structures of the bis[hydrotris(indazolyl)borato]metal complexes **4**−**8** indicate that even the very weak intermolecular C−H•••π interactions can be used to construct porous framework structures.

Experimental Section

The solvent, methanol, was dried with CaO by heating under reflux for 4 h under inert gas, followed by distillation. − UV/Vis spectra were obtained with a Jasco V-570, MHT-344 spectrometer in the range 1800−300 nm, and with a Polytec XDAP diode-array spectrometer with a quartz immersion probe in the range 1000−280 nm. NMR spectra were recorded with a Bruker ARX200 (200.1 MHz for ^{1}H, 50.3 MHz for ^{13}C), and calibrated against the solvent signal ([D_6]DMSO: ^{1}H NMR: δ = 2.53, ^{13}C NMR: δ = 39.5; $CDCl_3$: ^{1}H NMR: δ = 7.26, ^{13}C NMR: δ = 77.0; [D_8]THF: ^{1}H NMR: δ = 1.73, ^{13}C NMR: δ = 25.2; CD_3OD: ^{1}H NMR: δ = 3.31). The ^{11}B- and ^{10}B-NMR spectra were measured with a Bruker ARX200 (64.21 MHz for ^{11}B, 21.50 MHz for ^{10}B) relative to neat $BF_3 \bullet Et_2O$ as an external standard. A 1:2 v/v solvent mixture of [D_6]DMSO and normal DMSO was used with a sample concentration of about 130 mg/mL. Mass spectra were obtained with a Varian MAT 311A/AMD in solid-probe EI mode, at an ionization energy of 70 eV. The MS peaks listed refer to the most abundant isotope combination with ^{56}Fe, ^{59}Co, ^{58}Ni, ^{63}Cu, ^{54}Zn, and ^{11}B. Elemental analyses were carried out with a Perkin−Elmer 2400 Series II CHNS/O Analyzer. IR spectra were measured with a Nicolet Magna 750 as KBr disks.

Synthesis

Potassium Hydrotris(indazol-1-yl)borate, K[HB($C_7H_5N_2$)$_3$] (3): The potassium salt of **2a** was prepared following a general procedure by Trofimenko for tris(pyrazolyl)borate ligands:[51] KBH_4 (1.6 g, 30.0 mmol) and indazole (11.3 g, 95.9 mmol) were heated to 220 °C in a Schlenk flask that was connected to a volumetric gas measurement system. A strong gas evolution starts upon melting, and ceases towards the end of the reaction. After 4 h, 2.1 L of H_2 was evolved, which corresponds to 86.1 mmol or 96% when assuming the ideal gas law. Excess indazole was separated by sublimation (160 °C bath temperature, 1.5 mbar), to leave the product as a yellow powder (yield 10.57 g, 88%). NMR spectroscopy still showed indazole impurities that could not be removed, even after prolonged sublimation. The product was used as such for the following reactions with metal salts. M.p. 256−258 °C (ref.[12] 256−258 °C) − ^{1}H NMR (CD_3OD): 6.70−7.70 (m, 12 H, 4-, 5-, 6-, 7-H), 8.01 (s, 3 H, 3-H), the BH signal could not be observed; possibly due to its broad resonance because of quadrupolar coupling and relaxation effects from the boron atom.[52] − ^{13}C NMR (CD_3OD): δ = 113.8 (C-7), 120.3 (C-5), 121.0 (C-4), 125.7 (C-6), 125.8 (C-3a), 134.3 (C-3), 145.7 (C-7a) (the assignment of the quaternary C atoms C-3a and C-7a agrees with their lower signal intensity; the signals of the nitrogen-neighboring atoms C-3 and C-7a can be discerned by their low-field shift[7]). − ^{11}B NMR ([D_6]DMSO): δ = −3.5 (br), −9.3 (sh, assigned to the disubstituted borate), −35.6 (s, sharp signal, unchanged KBH_4). − ^{10}B NMR ([D_6]DMSO): δ = −5 (very broad with shoulder to high-field end), −35.6 (s, sharp signal, KBH_4). − MS (284 °C); *m/z* (%): 402 (4) $[M]^+$, 375 (4) $[M - HCN]^+$, 285 (20) $[M - C_7H_5N_2]^+$, 245 (12) $[B(C_7H_5N_2)_2]^+$, 118 (100) $[C_7H_6N_2]^+$, 91 (28) $[C_7H_6N_2 - HCN]^+$. − IR (KBr): $\tilde{\nu}$ = 3090 cm^{-1} w, 3056 w, 3038 w (νCH), 2440 w, 2416 w, 2382 w (νBH), 1615 m (νCN), 1574 m, 1496 m, 1459 m, 1436 sh, 1400 m, 1375 sh, 1364 w, 1337 m, 1263 m, 1209 w, 1155 s, 1110 s, 1024 sh, 1010 s, 994 m, 942 m, 908 s, 855 w, 835 m, 794 w, 787 w, 779 w, 759 s, 740 s, 663 m, 656 w, 646 w, 634 w, 622w, 609 w, 600 m, 569 w, 552 w, 458 w, 429 m.

[Bis{hydrotris(indazol-1-yl)borato]metal(II) Complexes, [M{HB($C_7H_5N_2$)$_3$}$_2$]. − General Procedure: A solution of **3** (400 mg, 1.0 mmol) in CH_3OH (10 mL) was added to a solution/slurry of the metal salt (0.5 mmol) in CH_3OH (5 mL) under stirring. The precipitate formed was filtered and dried in air. The product was separated from KCl by dissolution in THF, dioxane, or chloroform, followed by filtration. Crystallization was achieved either by cooling, overlayering with petroleum ether (30/50) or slow solvent evaporation. After crystallization, the crystals contained solvent of crystallization which in the case of $CHCl_3$ or THF was rapidly lost when removed from the mother liquor.

[Fe{HB($C_7H_5N_2$)$_3$}$_2$] (4): Starting material $(NH_4)_2Fe(SO_4)_2$. Pink to red needle-shaped crystals were initially obtained from chloroform under cooling to −15 °C. After 2 d at this temperature, the needles dissolved again and red rhombic crystals formed within another day. Yield 440 mg, 95%. − M.p. 446 °C (DSC). − ^{1}H NMR ($CDCl_3$): δ = 1.59 (s, br, 1 H, BH), 6.98 (t, 3 H, *J* = 7.2 Hz, 5-H), 7.35 (overlapping d and t, 6 H, *J* = 8.4 Hz, 6-H, 7-H), 7.42 (s, 3 H, 3-H), 8.15 (d, 3 H, *J* = 8.4 Hz, 4-H); ([D_8]THF): δ = 2.55 (s, br, 1 H, BH), 6.93 (t, 3 H, *J* = 7.5 Hz, 5-H), 7.34 (overlapping d and t, 6 H, *J* = 7.8, 8.3 Hz, 6-H, 7-H), 7.48 (s, 3 H, 3-H), 8.16 (d, 3 H, *J* = 8.4 Hz, 4-H). − ^{13}C NMR ([D_8]THF): δ = 111.2 (C-7), 119.8 (C-6), 120.5 (C-5), 126.0 (C-4), 126.3 (C-3a), 143.6 (C-3), 146.6 (C-7a). − MS (469 °C); *m/z* (%): 782 (68) $[M]^+$, 665 (46) $[M - C_7H_5N_2]^+$, 547 (7) $[M - 2(C_7H_5N_2) - H]^+$, 536 (19) $[M - 2(C_7H_5N_2) - BH]^+$, 419 (69) $[M - \{HB(C_7H_5N_2)_3\} = Fe\{HB(C_7H_5N_2)_3\}]^+$, 391 (5) $[M]^{2+}$, 332.5 (14) $[M - C_7H_5N_2]^{2+}$, 301 (86) $[Fe\{HB(C_7H_5N_2)_2\}]^+$, 274 (100) $[M - 2(C_7H_5N_2)]^{2+}$, 118 (55) $[C_7H_6N_2]^+$. − IR (KBr): $\tilde{\nu}$ = 3110 cm^{-1} w, 3064 w, 3039 w, 2905 w (νCH), 2490 sh, 2475 m (νBH), 1623 s, 1505 m, 1461 s, 1416 vs (νCN), 1378 sh, 1362 m, 1350 s, 1330 w, 1265 m, 1216 s, 1140 vs, 1135 sh, 1123 w, 1110 s, 1016 vs, 998 m, 920 m, 912 w, 848 m, 822 s, 757 vs, 740 vs, 726 s, 680 m, 597 m, 572 w, 560 w, 499 m, 440 m. − $C_{42}H_{32}B_2FeN_{12} \bullet (THF)_2$ (926.5): calcd. C 64.82, H 5.22, N 18.14; found C 64.24, H 5.28, N 16.06.

[Co{HB($C_7H_5N_2$)$_3$}$_2$] (5): Starting material $CoCl_2 \bullet 6\,H_2O$. An initial crystallization from dioxane/petroleum ether yielded red-brown needles and a yellow solid. The brown impurity could be removed after treatment of a $CHCl_3$ solution with Al_2O_3. This changed the relative solubility of the two phases. After evaporation of $CHCl_3$ in vacuum, the remaining solid was treated again with $CHCl_3$ (5 mL) which led to the dissolution of the brown impurity leaving a citrus-yellow solid behind. The yellow solid was crystallized from hot/cold $CHCl_3$ to give initially yellow needle-shaped crystals and after longer standing yellow rhombic crystals. Yield 220 mg, 56%. − M.p. > 300 °C. − ^{1}H NMR ($CDCl_3$): δ = +111.7 (1 H, BH),

+50.2 (3 H, 7-H), +20.1 (3 H, 6-H), +10.6 (3 H, 5-H), −9.9 (3 H, 4-H), −97.8 (3 H, 3-H); ([D$_6$]DMSO): δ = + 117 (1 H, BH), + 52.2 (3 H, 7-H), + 20.8 (3 H, 6-H), + 10.8 (3 H, 5-H), − 10.3 (3 H, 4-H), −101 (3 H, 3-H); ([D$_8$]THF): δ = + 117 (1 H, BH), + 52.1 (3 H, 7-H), + 20.7 (3 H, 6-H), + 10.7 (3 H, 5-H), −10.5 (3 H, 4-H), −102 (3 H, 3-H) (corresponds to ref.[12]). − MS (438 °C); *m*/*z* (%): 785 (83) $[M]^+$, 668 (76) $[M - C_7H_5N_2]^+$, 550 (16) $[M - 2(C_7H_5N_2) - H]^+$, 422 (69) $[M - \{HB(C_7H_5N_2)_3\} = Co\{HB(C_7H_5N_2)_3\}]^+$, 392.5 (3) $[M]^{2+}$, 334 (10) $[M - C_7H_5N_2]^{2+}$, 304 (67) $[Co\{HB(C_7H_5N_2)_2\}]^+$, 275.6 (100) $[M - 2(C_7H_5N_2)]^{2+}$, 118 (33) $[C_7H_6N_2]^+$. − IR (KBr): $\tilde{\nu}$ = 3103 cm^{-1} w, 3063 w (νCH), 2498 m, 2478 m (νBH), 1623 s, 1507 s (νCN), 1462 s, 1431 m, 1412 s, 1381 m, 1367 s, 1351 s, 1321 w, 1266 s, 1217 s, 1158 s, 1148 s, 1113 s, 999 s, 947 w, 916 s, 857 m, 835 s, 826 s, 760 vs, 748 s, 728 s, 666 s, 645 w, 599 s, 434 m. − $C_{42}H_{32}B_2CoN_{12}$ (785.35): calcd. C 64.23, H 4.11, N 21.40; found C 63.86, H 3.39, N 19.81. − $C_{42}H_{32}B_2CoN_{12} \cdot 4/3\ (CHCl_3)$ (944.5): calcd. C 55.10, H 3.56, N 17.80; found C 55.63, H 3.56, N 17.89.

[Ni{HB(C$_7$H$_5$N$_2$)$_3$}$_2$] (6): Starting material anhydrous $NiCl_2$. Light pink crystals from dioxane/petroleum ether or slow evaporation of THF. Yield 250 mg, 64%. M.p. > 300 °C − ^{1}H NMR ([D$_8$]THF): δ = 2.04 (s, 1 H, 3-H), 2.44 (s, 1 H, 4-H), 3.58 (s, 1 H, 5-H) 8.79 (br, s, 1 H, 6-H), 15.09 (br, s, 1 H, 7-H). − MS (428 °C); *m*/*z* (%): 784 (11) $[M]^+$, 667 (51) $[M - C_7H_5N_2]^+$, 549 (7) $[M - 2(C_7H_5N_2) - H]^+$, 421 (29) $[M - \{HB(C_7H_5N_2)_3\} = Ni\{HB(C_7H_5N_2)_3\}]^+$, 333.5 (4) $[M - C_7H_5N_2]^{2+}$, 304 (18) $[Ni\{HB(C_7H_5N_2)_2\}]^+$, 275 (27) $[M - 2(C_7H_5N_2)]^{2+}$, 118 (100) $[C_7H_6N_2]^+$. − IR (KBr): $\tilde{\nu}$ = 3237 cm^{-1} w, 3127 w, 3110 w, 3092 w, 3063 m, 3034 w, 2968 w, 2924 w (νCH), 2850 w, 2717 w, 2675 w, 2613 w, 2563 w, 2491 m, 2471 m (νBH),1937 w, 1903 w, 1880 w, 1789 w, 1686 w, 1682 w, 1622 s (νCN), 1566 w, 1504 s, 1461 s, 1430 m, 1409 s, 1378 m, 1362 s, 1347 s, 1322 w, 1284 w, 1263 s, 1213 m, 1185 w, 1155 s, 1144 s, 1137 s, 1124 w, 1111 s, 1066 w, 1040 m, 1014 s, 1003 sh, 994 s, 973 sh, 944 w, 938 w, 913 s, 909 sh, 850 m, 832 sh, 825 s, 815 w, 778 w, 765 sh, 756 s, 741 s, 723 s, 664 s, 646 w, 641 w, 596 s, 569 w, 556 w, 431 m. − $C_{42}H_{32}B_2N_{12}Ni$ (785.1): calcd. C 64.25, H 4.11, N 21.41; found C 63.89, H 3.68, N 20.01.

[Cu{HB(C$_7$H$_5$N$_2$)$_3$}$_2$] (7): Starting material anhydrous $CuCl_2$. Dark green crystals from hot/cold $CHCl_3$ or slow evaporation of THF. Yield 350 mg, 90%. M.p. > 300 °C. − ^{1}H NMR ([D$_8$]THF): δ = 6.7 (s, br $\omega_{1/2}$ = 130 Hz), 7.8 (s, br $\omega_{1/2}$ = 113 Hz), 9.2 (s, br $\omega_{1/2}$ = 74 Hz), 11.5 (s, br $\omega_{1/2}$ = 174 Hz). − MS (446 °C); *m*/*z* (%): 788 (0.5) $[M - H]^+$, 671 (14) $[M - C_7H_5N_2 - H]^+$, 555 (30) $[M - 2(C_7H_5N_2)]^+$, 426 (5) $[M - \{HB(C_7H_5N_2)_3\} = Cu\{HB(C_7H_5N_2)_3\}]^+$, 309 (67) $[Cu\{HB(C_7H_5N_2)_2\}]^+$, 282 (100) $[Cu\{HB(C_7H_5N_2)_2\} - HCN]^+$, 118 (33) $[C_7H_6N_2]^+$. − IR (KBr): $\tilde{\nu}$ = 3119 cm^{-1} w, 3067 m, 3043w (νCH), 2497 m, 2478 m (νBH), 1625 s, 1508 s, 1467 s (νCN), 1431 m, 1412 s, 1382 m, 1366 m, 1349 s, 1268 m, 1221 s, 1212 sh, 1159 s, 1147 s, 1139 m, 1114 s, 1044 m, 1024 s, 1012 s, 999 s, 943 w, 918 s, 911 sh, 855 m, 836 m, 827 s, 761 s, 742 s, 663 s, 644 w, 599 s, 435 m. − $C_{42}H_{32}B_2CuN_{12} \cdot 1/2\ (CHCl_3)$ (849.6): calcd. C 60.08, H 3.86, N 19.78; found C 59.63, H 3.90, N 19.47.

Table 6. Crystal data for compounds **4** • 3.5 $CHCl_3$, **5** • 3.5 $CHCl_3$, **6** • 3 THF, and **6** • 1.67 dioxane

Compound	**4** • 3.5 $CHCl_3$ [a]	**5** • 3.5 $CHCl_3$ [a]	**6** • 3 THF [a]	**6** • 1.67 dioxane
Empirical formula	$C_{45.5}H_{35.5}B_2Cl_{10.5}FeN_{12}$	$C_{45.5}H_{35.5}B_2Cl_{10.5}CoN_{12}$	$C_{54}H_{56}B_2N_{12}NiO_3$	$C_{48.67}H_{45.36}B_2N_{12}NiO_{3.33}$
M [g mol^{-1}]	1200.05	1203.13	1001.44	931.97
Crystal size [mm]	0.34×0.28×0.26	0.52×0.18×0.15	0.23×0.18×0.12	0.38×0.26×0.24
Crystal description	irregular	irregular	prismatic	irregular
Crystal color	red	yellow	pink	pink
T [K]	173(2)	173(2)	163(2)	173(2)
Diffractometer	Bruker AXS CCD	Bruker AXS CCD	Enraf-Nonius CAD4	Bruker AXS CCD
Scan type, 2Θ range	ω, 3.0−52°	ω, 3.0−52	ω−2Θ, 2.9−45	ω, 2.7−52°
h; *k*; *l* range	−28, 29; −24, 24; −27, 21	−28, 25; −24, 24; −28, 28	−1, 15; −16, 17; −12, 12	−37, 36; −37, 37; −16, 9
Crystal system	monoclinic	monoclinic	triclinic	trigonal
Space group	*C*2/*c*	*C*2/*c*	*P*−1	*R*−3
a [Å]	23.5337(6)	23.2237(2)	14.187(4)	30.2345(2)
b [Å]	19.7564(5)	19.9395(3)	15.989(4)	30.2345(2)
c [Å]	22.6844(6)	23.0847(4)	11.981(4)	13.2816(2)
α [°]	90	90	109.48(4)	90
β [°]	100.7230(10)	101.0840(10)	91.36(4)	90
γ [°]	90	90	77.98(4)	120
V [Å^3]	10362.71(5)	10490.4(3)	2503.0(13)	10514.45(19)
Z	8	8	2	9
$D_{calcd.}$ [g cm^{-3}]	1.538	1.524	1.297	1.317
F(000) [electrons]	4856	4864	1052	4374
μ [mm^{-1}]	0.88	0.909	0.444	0.472
Absorption correction	SADABS	SADABS	none	SADABS
min/max transmission	0.1817/0.4537	0.5612/0.8855		0.6040/1.0000
Measured reflections	33749	35010	6883	23784
Unique reflect. for refinemt (R_{int})	10149 (0.284)	10297(0.132)	6490(0.1485)	4600 (0.1299)
Observed reflections [$I > 2\sigma(I)$]	3563	5502	2176	2799
Parameters refined	649	649	652	303
max/min Δρ≅[b][e Å^{-3}]	1.113/−0.957	1.346/−1.018	0.436/−0.571	1.105/−0.492
*R*1/*wR2*[c][$I > 2\sigma(I)$]	0.0979/0.1725	0.0842/0.1631	0.1040/0.2339	0.0699/0.1526
*R*1/*wR2*[b] (all reflections)	0.2622/0.2191	0.1702/0.2014	0.2998/0.3323	0.1331/0.1853
GOF on F^2 [c]	1.006	1.005	0.953	1.027
Weighting scheme *w*; *a*/*b*[d]	0.0465/0.0000	0.0661/60.1354	0.1550/1.9761	0.0761/39.6694

[a] Two independent molecules in the unit cell. − [b] Largest difference peak and hole. − [c] $R1 = (\Sigma||F_o| - |F_c||)/\Sigma|F_o|$; $wR2 = \{\Sigma[w(F_o^2 - F_c^2)^2]/\Sigma[w(F_o^2)^2]\}^{1/2}$ − [d] Goodness-of-fit, Gof = $\{\Sigma[w(F_o^2 - F_c^2)^2]/(n - p)\}^{1/2}$; $w = 1/[\sigma^2(F_o^2) + (a \cdot P)^2 + b \cdot P]$ where $P = [\max(F_o^2 \text{ or } 0) + 2 \cdot F_c^2]/3$.

[Zn{HB($C_7H_5N_2$)$_3$}$_2$] (8): Starting material $Zn(O_2CCH_3)_2 \cdot 2\,H_2O$. White, needle-shaped crystals from dioxane/petroleum ether (diffusion method). Yield 280 mg, 71%. M.p. > 300 °C − ^{1}H NMR ([D$_6$]DMSO): δ = 7.09 (t, 1 H, *J* = 7.4 Hz, 5-H), 7.52 (t, 1 H, *J* = 7.6 Hz, 6-H), 7.63 (d, 1 H, *J* = 8.0 Hz, 7-H), 7.79 (s, 1 H, 3-H), 8.30 (d, 1 H, *J* = 8.5 Hz, 4-H); ([D$_8$]THF): δ = 7.05 (td, 1 H, *J* = 7.6, 0.8 Hz, 6-H), 7.45 (td, 1 H, *J* = 7.7, 1.1 Hz, 5-H), 7.56 (dt, 1 H, *J* = 8.1, 0.9 Hz, 7-H), 7.78 (d, 1 H, *J* = 0.9 Hz, 3-H), 8.25 (dd, 1 H, *J* = 8.7, 0.9 Hz, 4-H4). − ^{13}C NMR ([D$_8$]THF): δ = 112.9 (C-7), 121.3 (C-6), 121.8 (C-5), 123.9 (C-4), 127.7(C-3a), 134.7 (C-3), 144.6 (C-7a). − MS (441 °C); *m*/*z* (%): 790 (9) $[M]^+$, 673 (100) $[M - C_7H_5N_2]^+$, 555 (10) $[M - 2\,(C_7H_5N_2) - H]^+$, 544 (9) $[M - 2\,(C_7H_5N_2) - BH]^+$, 427 (34) $[M - \{HB(C_7H_5N_2)_3\} = Zn\{HB(C_7H_5N_2)_3\}]^+$, 336.5 (5) $[M - C_7H_5N_2]^{2+}$, 309 (73) $[Zn\{HB(C_7H_5N_2)_2\}]^+$, 278 (84) $[M - 2\,(C_7H_5N_2)]^{2+}$, 118 (33) $[C_7H_6N_2]^+$. − IR (KBr): $\tilde{\nu}$ = 3084 cm^{-1} w, 3066 w, 3033 w (νCH), 2487 w, 2470 m (νBH), 1938 w, 1903 w, 1621 s (νCN), 1504 s, 1461 s, 1426 m, 1406 s, 1378 m, 1357 m, 1345 s, 1320 w, 1261 s, 1212 m, 1156 s, 1145 s, 1137 s, 1113 s, 1038 m, 1014 s, 995 s, 937 w, 912 m, 908 m, 842 w, 824 s, 816 s, 776 w, 755 s, 739 s, 733 s, 730 s, 686 w, 661 s, 641 w, 597 s, 568 w, 554 w, 431 m. − $C_{42}H_{32}B_2N_{12}Zn$ (791.8): calcd. C 63.71, H 4.07, N 21.23; found C 63.48, H 3.15, N 21.01.

Electrochemical Measurements: All electrochemical experiments were carried out in specially constructed cells containing an internal drying column with highly activated alumina. The working electrode was a Pt disk sealed in soft glass (1.00 mm diameter). A Pt wire, wrapped around the glass of the working electrode, was used as the counter electrode. The reference electrode was an Ag wire on which AgCl had been deposited electrolytically. Potentials were calibrated with ferrocene (+0.352 V vs. Ag/AgCl). The measurements were performed with a Jaissle Potentiostat IMP 88 and a PAR 175 programmer.

Mössbauer Spectroscopy: ^{57}Fe-Mössbauer spectra were measured in constant acceleration modus with a triangular velocity profile [accelerator, control unit and multichannel analyzer (1024 data channels) from WISSEL]. The ^{57}Co source in an Rh matrix (AMERSHAM) had an activity of about 115 MBq. The Mössbauer transition at 14.41 keV was used for the γ-radiation. The transmission of the γ-radiation was detected by means of an NaI (Tl) scintillation counter as the detector coupled with a secondary electron multiplier (HARSHAW/ELSCINT); amplifier and energy discriminator from INTERTECHNIQUE. The experimental spectra were iteratively approximated in a least-squares fit with Lorentz functions in the thin absorber approximation (program package NORMOS).[53] Singlets were fitted with a single Lorentz curve, doublets with a symmetric or asymmetric superposition of two Lorentz functions. The spectral parameters ($\delta^{\alpha-Fe}$, Γ/2, and possibly ΔE_Q) could each be fixed or correlated in groups in the case of a multi-line fit. Fits were aimed for with largely open parameters. The $\delta^{\alpha-Fe}$ scale of the isomer shift is related to the shift of α-iron as origin of the ordinate ($\delta^{\alpha-Fe}$ = 0.11 ± 0.01 mm/s + $\delta^{Fe/Rh}$). The iron contamination in the beam, especially in the beryllium windows of the detector was taken into account with two fixed

Table 7. Crystal data for compounds **7** • 1.33 $CHCl_3$, **7** • 2.5 THF, and **8** • 1.67 dioxane

Compound	**7** • 1.33 $CHCl_3$[a]	**7** • 2.5 THF	**8** • 1.67 dioxane
Empirical formula	$C_{43.33}H_{33.33}B_2Cl_4CuN_{12}$	$C_{52}H_{52}B_2CuN_{12}O_{2.5}$	$C_{48.67}H_{45.36}B_2N_{12}O_{3.33}Zn$
M [g mol^{-1}]	949.11	970.22	938.66
Crystal size [mm]	0.40×0.38×0.18	0.5×0.4×0.2	0.32×0.32×0.21
Crystal description	irregular	prism	plate
Crystal color	dark green	dark green	colorless
T [K]	173(2)	163(2)	180(2)
Diffractometer	Bruker AXS CCD	Enraf-Nonius CAD4	Bruker AXS CCD
Scan type, 2Θ range	ω, 2.9−54	ω-2Θ, 3.4−55°	ω, 2.7−46.5°
h; *k*; *l* range	−16, 16; −15, 19 −18, 23	0, 21; 0, 21; 0, 21	−33, 33; −33, 33; −14, 14
Crystal system	triclinic	tetragonal	trigonal
Space group	*P*−1	$P4_2/n$	*R*−3
a [Å]	13.2637(3)	16.779(5)	30.3636(8)
b [Å]	15.0498(3)	16.779(5)	30.3636(8)
c [Å]	18.5660(4)	16.538(5)	13.1960(5)
α [°]	68.6800(10)	90	90
β [°]	72.8510(10)	90	90
γ [°]	88.4900(10)	90	120
V [Å^3]	3285.32(12)	4656(2)	10536.1(6)
Z	3	4	9
$D_{calcd.}$ [g cm^{-3}]	1.439	1.355	1.312
F(000) [electrons]	1453	2028	4392
μ [mm^{-1}]	0.791	0.526	0.581
Absorption correction	SADABS	none	none
min/max transmission	0.4307/0.5035		
Measured reflections	24328	5704	24730
Unique reflect. for refinemt (R_{int})	14170 (0.0578)	5346 (0.0569)	3373 (0.0636)
Observed reflection [$I > 2\sigma(I)$]	8615	2871	2601
Parameters refined	847	341	273
max/min Δρ≅[b][e Å^{-3}]	0.532/−0.630	0.696/−0.742	0.891/−0.356
*R*1/*wR*2[c][$I > 2\sigma(I)$]	0.0489/0.961	0.0662/0.1861	0.0465/0.1276
*R*1/*wR*2[b] (all reflections)	0.1004/0.1119	0.1463/0.2217	0.0631/0.1388
GOF on F^2 [c]	1.006	1.033	1.033
Weighting scheme *w*; *a*/*b*[d]	0.0256/0.0000	0.1288/0.0000	0.0819/20.9372

[a] Two independent molecules in the unit cell. − [b] Largest difference peak and hole. − [c] $R1 = (\Sigma||F_o| - |F_c||)/\Sigma|F_o|$; $wR2 = \{\Sigma[w(F_o^2 - F_c^2)^2]/\Sigma[w(F_o^2)^2]\}^{1/2}$ − [d] Goodness-of-fit, Gof = $\{\Sigma\,[w(F_o^2 - F_c^2)^2]/(n - p)\}^{1/2}$; $w = 1/[\sigma^2(F_o^2) + (a \cdot P)^2 + b \cdot P]$ where $P = [\max(F_o^2 \text{ or } 0) + 2 \cdot F_c^2]/3$.

base lines. The sample was heated under vacuum to collect the high-temperature spectra.

X-ray Structure Determinations: Data were collected with Mo-K_α radiation (λ = 0.71073 Å) and the use of a graphite monochromator. Structure solution was performed by direct methods; refinement was done by full-matrix least squares on F^2 using the SHELXTL program package (Version 5.1, Bruker AXS). All non-hydrogen positions were found and refined. The atoms were refined with anisotropic temperature factors except for the disordered dioxane solvent molecules in **6** • 1.67 dioxane and **8** • 1.67 dioxane and part of the THF solvent in **7** • 3 THF. The hydrogen atoms on the indazolyl rings and on the boron atom were placed at calculated positions, using appropriate riding models and an isotropic temperature factor of B_{eq} = 0.08 [for **8** • 1.67 dioxane B_{eq}(H) = 1.2 B_{eq}(C)]. For **6** • 1.67 dioxane and **8** • 1.67 dioxane the hydrogen position on the boron atom was found and refined. For the THF and dioxane solvent molecules no hydrogen atom positions were calculated or only on less disordered moieties. Crystal data are listed in Table 6 and 7. Graphics were computed with ORTEP3 for Windows.[54] Special computations for the crystal structure discussions were carried out with PLATON for Windows.[55] Crystallographic data (excluding structure factors) for the structures reported in this paper have been deposited with the Cambridge Crystallographic Data Center as supplementary publication No. CCDC-136881 (**4** • 3.5 $CHCl_3$), -136882 (**5** • 3.5 $CHCl_3$), -136883 (**6** • 3 THF), -136884 (**6** • 1.67 dioxane), -136885 (**7** • 1.33 $CHCl_3$), -136886 (**7** • 3 THF), -136887 (**8** • 1.67 dioxane). Copies of the data can be obtained free of charge on application to CCDC, 12 Union Road, Cambridge CB2 1EZ, UK [Fax: int. code + 44-1223/336-033; E-mail: deposit@ccdc.cam.ac.uk]. A full listing of the intermolecular C−H•••π contacts [C−H•••C < 3.1 Å, C−H•••centroid < 3.4 Å (distances and angles)] and of the ring-centroid−ring-centroid contacts (< 6.0 Å) can be found in the supporting information.

Acknowledgments

This work is supported by the Deutsche Forschungsgemeinschaft (grant Ja466/4-2, 4-3 and grant Ja466/10-1), the Fonds der Chemischen Industrie, and the Graduiertenkolleg "Unpaired Electrons" at the University of Freiburg.

[1] The abbreviation Tp^{4Bo} for hydrotris(indazol-1-yl)borate follows the suggested nomenclature by S. Trofimenko[3] to indicate the relationship to the pyrazole-derived Tp-class of ligands; "4Bo" indicates the 4,5-fusion of the benzo ring.

[2] S. Trofimenko, *J. Am. Chem. Soc.* **1967**, *89*, 3170−3177.

[3] Reviews: S. Trofimenko, *Scorpionates−Polypyrazolylborate Ligands and Their Coordination Chemistry*, Imperial College Press, **1999**. S. Trofimenko, *Chem. Rev.* **1993**, *93*, 943−980. P. K. Byers, A. J. Canty, R. T. Honeyman, *Adv. Organomet. Chem.* **1992**, *34*, 1−65. N. Kitajima, W. B. Tolman, *Prog. Inorg. Chem.* **1995**, *43*, 419. G. Parkin, *Adv. Inorg. Chem.* **1995**, *42*, 291−393. D. L. Reger, *Coord. Chem. Rev.* **1996**, *147*, 571−595. M. Etienne, *Coord. Chem. Rev.* **1997**, *156*, 201−236. C. Janiak, *Main Group Met. Chem.* **1998**, *21*, 33−49.

[4] Recent examples of inorganic Tp−metal complexes: Y. Takahashi, S. Hikichi, M. Akita, Y. Moro-oka, *Chem. Commun.* **1999**, 1491−1492. C. Janiak, L. Braun, F. Girgsdies, *J. Chem. Soc., Dalton Trans.* **1999**, 3133−3136. J. L. Kisko, T. Hascall, C. Kimblin, G. Parkin, *J. Chem. Soc., Dalton Trans.* **1999**, 1929−1935. R. L. Paul, A. J. Amoroso, P. L. Jones, S. M. Couchman, Z. R. Reeves, L. H. Rees, J. C. Jeffery, J. A. McCleverty, M. D. Ward, *J. Chem. Soc., Dalton Trans.* **1999**, 1563−1568. F. Malbosc, P. Kalck, J.-C. Daran, M. Etienne, *J. Chem. Soc., Dalton Trans.* **1999**, 271−272. C. Santini, G. G. Lobbia, C. Pettinari, M. Pellei, G. Valle, S. Calogero, *Inorg. Chem.* **1998**, *37*, 890−900. J. S. Fleming, E. Psillakis, S. M. Couchman, J. C. Jeffrey, J. A. McCleverty, M. D. Ward, *J. Chem. Soc., Dalton Trans.* **1998**, 537−543. M. H. W. Lam, Y.-Y. Tang, K.-M. Fung, X.-Z. You, W.-T. Wong, *Chem. Commun.* **1997**, 957−958. C. Janiak, S. Temizdemir, T. G. Scharmann, *Z. Anorg. Allg. Chem.* **1998**, *624*, 755−756.

[5] Recent examples of bioinorganic Tp−metal complexes: M. A. Halcrow, L. M. L. Chia, X. Liu, E. J. L. McInnes, L. J. Yellowless, F. E. Mabbs, I. J. Scowen, M. McPartlin, J. E. Davies, *J. Chem. Soc., Dalton Trans.* **1999**, 1753−1762. H. Komatsuzaki, Y. Nagasu, K. Suzuki, T. Shibasaki, M. Satoh, F. Ebina, S. Hikichi, M. Akita, Y. Moro-oka, *J. Chem. Soc., Dalton Trans.* **1998**, 511−512.

[6] C. Janiak, T. G. Scharmann, W. Günther, W. Hinrichs, D. Lentz, *Chem. Ber.* **1996**, *129*, 991−995. C. Janiak, T. G. Scharmann, P. Albrecht, F. Marlow, R. MacDonald, *J. Am. Chem. Soc.* **1996**, *118*, 6307−6308. C. Janiak, T. G. Scharmann, W. Günther, F. Girgsdies, H. Hemling, D. Lentz, *Chem. Eur. J.* **1995**, *1*, 637−644.

[7] C. Janiak, T. G. Scharmann, H. Hemling, D. Lentz, J. Pickardt, *Chem. Ber.* **1995**, *128*, 235−244.

[8] C. Janiak, T. G. Scharmann, J. C. Green, R. P. G. Parkin, M. J. Kolm, E. Riedel, W. Mickler, J. Elguero, R. M. Claramunt, D. Sanz, *Chem. Eur. J.* **1996**, *2*, 992−1000.

[9] C. Janiak, T. G. Scharmann, T. Bräuniger, J. Holubová, M. Nádvorník, *Z. Anorg. Allg. Chem.* **1998**, *624*, 769−774.

[10] C. Janiak, T. G. Scharmann, K.-W. Brzezinka, P. Reich, *Chem. Ber.* **1995**, *128*, 323−327. C. Janiak, L. Esser, *Z. Naturforsch.* **1993**, *48B*, 394−396.

[11] H. V. R. Dias, W. Jin, *Inorg. Chem.* **1996**, *35*, 3687−3694. H. V. R. Dias, W. Jin, H.-J. Kim, H.-L. Lu, *Inorg. Chem.* **1996**, *35*, 2317−2328.

[12] A. L. Rheingold, G. Yap, S. Trofimenko, *Inorg. Chem.* **1995**, *34*, 759−760.

[13] A. L. Rheingold, B. S. Haggerty, G. P. A. Yap, S. Trofimenko, *Inorg. Chem.* **1997**, *36*, 5097−5103.

[14] A. L. Rheingold, L. M. Liable-Sands, G. P. A. Yap, S. Trofimenko, *Chem. Commun.* **1996**, 1233−1234.

[15] A. L. Rheingold, B. S. Haggerty, S. Trofimenko, *Chem. Commun.* **1994**, 1973−1974.

[16] F. J. Lalor, S. M. Miller, N. Garvey, *Polyhedron* **1990**, *9*, 63−68.

[17] K. S. Siddiqi, M. A. Neyazi, S. A. A. Zaidi, *Synth. React. Inorg. Met.-Org. Chem.* **1981**, *11*, 253−265. S. A. A. Zaidi, M. A. Neyazi, *Trans. Met. Chem.* **1979**, *4*, 164−167.

[18] C. Janiak, *Chem. Ber.* **1994**, *127*, 1379−1385.

[19] J. P. Jesson, S. Trofimenko, D. R. Eaton, *J. Am. Chem. Soc.* **1967**, *89*, 3158−3164.

[20] J. P. Jesson, S. Trofimenko, D. R. Eaton, *J. Am. Chem. Soc.* **1967**, *89*, 3148−3158.

[21] J. P. Jesson, *J. Chem. Phys.* **1966**, *45*, 1049−1056.

[22] A. Fruchier, E. Alcalde, J. Elguero, *Org. Magn. Res.* **1977**, *9*, 235−236. J. Elguero, A. Fruchier, M. C. Pardo, *Can. J. Chem.* **1976**, *54*, 1329−1330.

[23] C. K. Jørgensen, *Modern Aspects of Ligand Field Theory*, Elsevier, New York, **1971**, chapter 26.

[24] Reviews: P. Gütlich, A. Hauser, H. Spiering, *Angew. Chem.* **1994**, *106*, 2109−2141; *Angew. Chem. Int. Ed. Engl.* **1994**, *33*, 2024−2054. O. Kahn, Molecular Magnetism, VCH, Weinheim, **1993**, chapter 4, p. 53ff. J. Zarembowitch, *New. J. Chem.* **1992**, *16*, 255−267. P. Gütlich, A. Hauser, *Coord. Chem. Rev.* **1990**, *97*, 1−22. H. Toftlund, *Coord. Chem. Rev.* **1989**, *94*, 67−108. E. König, *Progr. Inorg. Chem.* **1987**, *35*, 527−622. P. Gütlich, *Struct. Bonding (Berlin)* **1981**, *44*, 83−195. H. A. Goodwin, *Coord. Chem. Rev.* **1976**, *18*, 293−325.

[25] S. Zamponi, G. Gambini, P. Conti, G. G. Lobbia, R. Marassi, M. Berrettoni, B. Cecchi, *Polyhedron* **1995**, *14*, 1929−1935. T. Buchen, P. Gütlich, *Inorg. Chim. Acta* **1995**, *231*, 221−223. J.-P. Martin, J. Zarembowitch, A. Dworkin, J. G. Haasnoot, E. Codjovi, *Inorg. Chem.* **1994**, *33*, 2617−2623.

[26] F. Grandjean, G. J. Long, B. B. Hutchinson, L. Ohlhausen, P. Neill, J. D. Holcomb, *Inorg. Chem.* **1989**, *28*, 4406−4414.

[27] S. Calogero, G. G. Lobbia, P. Cecchi, G. Valle, J. Friedl, *Polyhedron* **1994**, *13*, 87−97.

[28] Y. Sohrin, H. Kokusen, M. Matsui, *Inorg. Chem.* **1995**, *34*, 3928−3934.

[29] G. J. Long, B. B. Hutchinson, *Inorg. Chem.* **1987**, *26*, 608−613.

A. Gulino, E. Ciliberto, S. Di Bella, I. Fragalà, *Inorg. Chem.* **1993**, *32*, 3759−3761. B. Hutchinson, L. Daniels, E. Henderson, P. Neill, G. J. Long, L. W. Becker, *J. Chem. Soc., Chem. Commun.* **1979**, 1003−1004. J. P. Jesson, J. F. Weiher, S. Trofimenko, *J. Chem. Phys.* **1968**, *48*, 2058−2066. J. P. Jesson, J. F. Weiher, *J. Chem. Phys.* **1967**, *46*, 1995−1996.

[30] Tp_2Fe: J D. Oliver, D. F. Mullica, B. B. Hutchinson, W. O. Milligan, *Inorg. Chem.* **1980**, *19*, 165−169.

[31] Tp_2Co: M. R. Churchill, K. Gold, C. E. Maw, Jr., *Inorg. Chem.* **1970**, *9*, 1597−1605.

[32] Tp_2Cu: A. Murphy, B. J. Hathaway, T. J. King, *J. Chem. Soc., Dalton Trans.* **1979**, 1646−1650.

[33] Tp_2Zn: K. Nakata, S. Kawabata, K. Ichikawa, *Acta Crystallogr.* **1995**, *C51*, 1092−1094.

[34] Tp'_2Fe and Tp'_2Co: C. Janiak, *Chem. Commun.* **1994**, 545−547

[35] Tp'_2Zn: C. Janiak, H. Hemling, *J. Chem. Soc., Dalton Trans.* **1994**, 2947−2952.

[36] A. G. Orpen, L. Brammer, F. H. Allen, O. Kennard, D. G. Watson, R. Taylor, *J. Chem. Soc., Dalton Trans.* **1989**, S1-S83.

[37] C. Janiak, *Moderne Anorganische Chemie* (Ed.: E. Riedel), de Gruyter, Berlin **1999**, p. 204. J. E. Huheey, E. A. Keiter, R. L. Keiter, *Inorganic Chemistry*, HarperCollins **1993**, p. 408ff.

[38] Selected recent examples: C. Janiak, S. Deblon, H.-P. Wu, M. J. Kolm, P. Klüfers, H. Piotrowski, P. Mayer, *Eur. J. Inorg. Chem.* **1999**, 1507−1521. M. P. Lightfoot, F. S. Mair, R. G. Pritchard, J. E. Warren, *Chem. Commun.* **1999**, 1945−1946. C. Bonnefous, N. Bellec, R. P. Thummel, *Chem. Commun.* **1999**, 1243−1244. S. Noro, M. Kondo, T. Ishii, S. Kitagawa, H. Matsuzaka, *J. Chem. Soc., Dalton Trans.* **1999**, 1569−1574. A. Bernardo, F. Pina, B. Escuder, E. Garcia-España, L. Godino-Salido, J. Latorre, S. V. Luis, J. A. Ramirez, C. Soriano, *J. Chem. Soc., Dalton Trans.* **1999**, 915−921. H.-P. Wu, C. Janiak, L. Uehlin, P. Klüfers, P. Mayer, *Chem. Commun.* **1998**, 2637−2638. E. Ishow, A. Gourdon, J.-P. Launay, *Chem. Commun.* **1998**, 1909−1910. N. Yoshida, H. Oshio, T. Ito, *Chem. Commun.* **1998**, 63−64.

[39] D. B. Amabilino, J. F. Stoddart, *Chem. Rev.* **1995**, *95*, 2725−2828. T. Dahl, *Acta Chem. Scand.* **1994**, *48*, 95−106.

[40] C. A. Hunter, *Chem. Soc. Rev.* **1994**, 101−109. C. A. Hunter, J. K. M. Sanders, *J. Am. Chem. Soc.* **1990**, *112*, 5525−5534.

[41] R. L. Jaffe, G. D. Smith, *J. Chem. Phys.* **1996**, *105*, 2780−2788.

[42] P. Hobza, H. L. Selzle, E. W. Schlag, *Chem. Rev.* **1994**, *94*, 1767−1785.

[43] F. Cozzi, J. S. Siegel, *Pure Appl. Chem.* **1995**, *67*, 683−689.

[44] E. G. Cox, D. W. Cruickshank, J. A. S. Smith, *Proc. R. Soc. London, Ser. A* **1958**, *247*, 1−20

[45] N. N. L. Madhavi, A. K. Katz, H. L. Carrell, A. Nangia, G. R. Desiraju, *Chem. Commun.* **1997**, 1953−1954. H.-C. Weiss, D. Bläser, R. Boese, B. M. Doughan, M. M. Haley, *Chem. Commun.* **1997**, 1703−1704. T. Steiner, M. Tamm, B. Lutz, J. van der Maas, *Chem. Commun.* **1996**, 1127−1128. P. L. Anelli, P. R. Ashton, R. Ballardini, V. Balzani, M. Delgado, M. T. Gandolfi, T. T. Goodnow, A. E. Kaifer, D. Philp, M. Pietraszkiewicz, L. Prodi, M. V. Reddington, A. M. Z. Slawin, N. Spencer, J. F. Stoddart, C. Vicent, D. J. Williams, *J. Am. Chem. Soc.* **1992**, *114*, 193−218.

[46] Other recent examples of supramolecular design involving C−H•••π interactions: B. J. McNelis, L. C. Nathan, C. J. Clark, *J. Chem. Soc., Dalton Trans.* **1999**, 1831−1834. K. Biradha, C. Seward, M. J. Zaworotko, *Angew. Chem. Int. Ed.* **1999**, *38*, 492−495.

[47] H.-P. Wu, C. Janiak, G. Rheinwald, H. Lang, *J. Chem. Soc., Dalton Trans.* **1999**, 183−190.

[48] G. Baum, E. C. Constable, D. Fenske, C. E. Housecroft, T. Kulke, *Chem. Commun.* **1998**, 2659−2660.

[49] C. Janiak, *Chem. Ber.* **1993**, *126*, 1603−1607.

[50] R. Pinalli, F. F. Nachtigall, F. Ugozzoli, E. Dalcanale, *Angew. Chem. Int. Ed.* **1999**, *38*, 2377−2380.

[51] S. Trofimenko, *Inorg. Synth.* **1970**, *12*, 99−106.

[52] R. K. Harris, *Nuclear Magnetic Resonance Spectroscopy*, Pitman, London, **1983**, chapters 5−14, pp. 138−141.

[53] R. A. Brand, University of Duisburg, Dept. of Applied Physics, **1992** (Distribution through WISSEL, Starnberg, Germany).

[54] M. N. Burnett, C. K. Johnson, *ORTEP-III*: Oak Ridge Thermal Ellipsoid Plot Program for Crystal Structure Illustrations, Oak Ridge National Laboratory Report ORNL-6895, **1996**. L. J. Farrugia, *ORTEP3 for Windows*, version 1.0.1β, University of Glasgow, Scotland, **1997**.

[55] A. L. Spek, *Acta Crystallogr.* **1990**, *A46*, C34; *PLATON* Version 29−11−98. Windows implementation: L. J. Farrugia, University of Glasgow, Scotland, **1998**.

Received November 29, 1999
[I99436]